Phys. Status Solidi A **209**, No. 10, 1861–1865 (2012) / **DOI** 10.1002/pssa.201200360

physica status solidi a
www.pss-a.com
applications and materials science

Part of Topical Section on
Advanced Silicon Materials for Electronics and Photovoltaics

Engineering metal precipitate size distributions to enhance gettering in multicrystalline silicon

Jasmin Hofstetter*,[1], David P. Fenning[1], Jean-François Lelièvre[2], Carlos del Cañizo[3], and Tonio Buonassisi[1]

[1] Massachusetts Institute of Technology, 77 Massachusetts Ave., Cambridge MA, 02139, USA
[2] Universidad Politécnica de Madrid, Avd. Complutense s/n, 28040 Madrid, Spain
[3] Centro de Tecnología del Silicio Solar CENTESIL, Getafe, Spain

Received 12 June 2012, revised 17 July 2012, accepted 18 July 2012
Published online 20 August 2012

Keywords defect engineering, gettering, silicon solar cells, simulation

* Corresponding author: e-mail jasmin.hofstetter@gmx.de, Phone: +1 617 452 2224, Fax +1 617 253 1556

The extraction of metal impurities during phosphorus diffusion gettering (PDG) is one of the crucial process steps when fabricating high-efficiency solar cells using low-cost, lower-purity silicon wafers. In this work, we show that for a given metal concentration, the size and density of metal silicide precipitates strongly influences the gettering efficacy. Different precipitate size distributions can be already found in silicon wafers grown by different techniques. In our experiment, however, the as-grown distribution of precipitated metals in multicrystalline Si sister wafers is engineered through different annealing treatments in order to control for the concentration and distribution of other defects. A high density of small precipitates is formed during a homogenization step, and a lower density of larger precipitates is formed during extended annealing at 740 °C. After PDG, homogenized samples show a decreased interstitial iron concentration compared to as-grown and ripened samples, in agreement with simulations.

© 2012 WILEY-VCH Verlag GmbH & Co. KGaA, Weinheim

1 Introduction A new generation of kerfless Si wafer materials is evolving with the potential advantage of being more cost-effective than ingot-grown wafers mainly due to reduced energy consumption and material loss during growth [1]. With the variety of silicon-based materials growing, a deeper understanding of the optimum processing regimes available to each – and the defects that limit them during processing – is required to produce the highest efficiencies and to compete in the difficult solar market.

For example, it is known that ingot- and ribbon-grown wafer materials respond differently to solar cell processing, in particular to phosphorus diffusion gettering (PDG) [2, 3]. Generally, the improvement of material performance during industrial PDG processes seems to be more pronounced on ingot-grown materials than on ribbon wafers. One reason for the different response is the large variation of impurity and structural defect concentrations that can be found in different materials [4, 5]. A second reason, however, might be different size distributions of metal-silicide precipitates that have been found by X-ray fluorescence microscopy studies [6]. One of the main reasons for varying metal silicide size distributions is the different cooling rates after crstyallization for different materials and growth methods. The formation of different size distributions as a function of the cooling rate and of available precipitate nucleations sites has been modeled by Haarahiltunen et al. [7].

It was first suggested through simulations by Plekhanov et al. [8] that the gettering efficacy strongly depends on precipitate size and density in the as-grown wafer. In this work, we perform a computational and experimental study the efficacy of PDG as a function of the average size distribution of metal-silicide precipitates in the as-grown material. In the following, with the help of simulation, we first study the kinetics and evolution of iron interstitials, Fe_i, and iron-silicide precipitates during PDG for different average precipitate sizes. Then, we test our theoretical findings experimentally. The precipitate size distribution in a set of multi-crystalline Si (mc-Si) sister wafers is manipulated by means of pre-annealing treatments. Finally, the reduction of the Fe_i concentration after PDG in the different wafers is tested.

© 2012 WILEY-VCH Verlag GmbH & Co. KGaA, Weinheim

2 Simulation The concentration evolution of precipitated and interstitial iron during PDG was simulated with the help of the *I2E* simulation tool [9, 10], a freely accessible online applet. The underlying model accounts for the in-diffusion of P into the Si, the dissolution and growth of precipitates, and the diffusion and segregation of interstitially dissolved iron atoms, Fe_i, to the P-diffused layer as a function of the applied time-temperature profile.

A PDG step of 40 min at 840 °C followed by a 10 min ramp to 800 °C and finally, an exponential cooldown to room temperature with a time constant of 6 min was simulated. As initial conditions, a total iron concentration of $2 \times 10^{14}\,cm^{-3}$, an interstitial iron concentration of $5 \times 10^{11}\,cm^{-3}$ and an as-grown precipitate radius of 16, 19, and 21 nm, respectively, were assumed.

2.1 Iron concentration evolution during PDG Figure 1a shows the simulated evolution of the average Fe_i concentration in the wafer bulk as a function of time during PDG for three different as-grown precipitate radii, r_0. The corresponding precipitate densities, N, have been calculated by dividing the total iron concentration by the number of iron atoms per precipitate and are also given. The solid solubility of iron in Si at 840 °C is about $1 \times 10^{13}\,cm^{-3}$ [11], much higher than the Fe_i concentration in the as-grown wafer. Consequently, iron-silicide precipitates instantly start dissolving during the high temperature step and in all three cases the Fe_i concentration increases from its as-grown value up to concentrations above $1 \times 10^{12}\,cm^{-3}$. However, before the solid solubility concentration is reached, the Fe_i concentration starts to decrease after a few minutes. This decrease is due to gettering of interstitially dissolved iron to the P-diffused layer. A quasi steady-state equilibrium of the average bulk Fe_i concentration is established, determined by a balance between dissolution of iron-silicide precipitates and gettering of interstitially dissolved iron. During cooldown after the 40 min PDG step, a sharp drop in the Fe_i concentration is observed. The solid solubility of iron in Si decreases with decreasing temperature and at the same time, the segregation coefficient in the P-diffused layer increases. This results in a higher driving force for interstitially dissolved iron to diffuse toward and segregate in the P-diffused layer so that the average bulk Fe_i concentration is significantly reduced during cooldown.

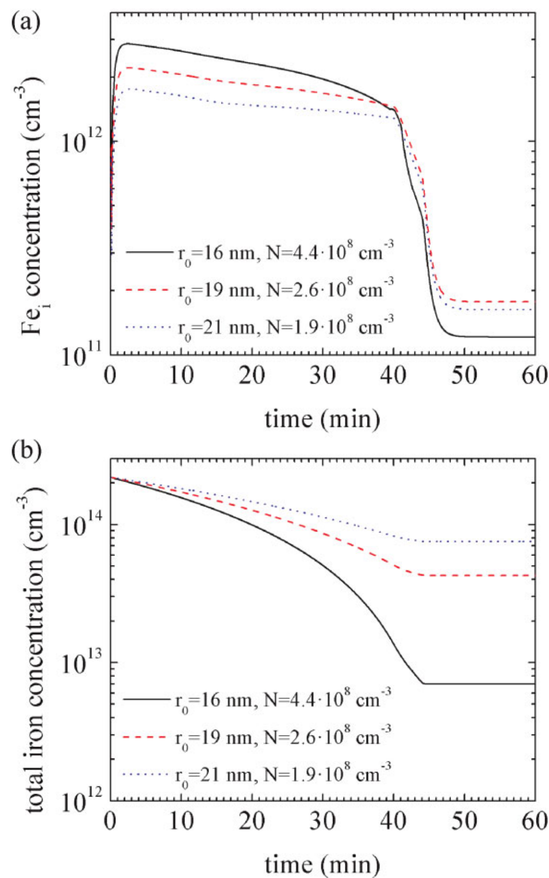

Figure 1 (online color at: www.pss-a.com) Simulated evolution of (a) the average Fe_i concentration and (b) the total iron concentration in the wafer bulk as a function of time during 40 min PDG at 840 °C followed by a 10 min ramp to 800 °C and an exponential cooldown to room temperature for three different as-grown precipitate radii, r_0; corresponding precipitate densities, N, are also given.

Figure 1b shows the simulated evolution of the average total iron concentration in the wafer bulk as a function of time during PDG for three different as-grown precipitate radii. The iron concentration steadily decreases with time for all three cases. But it decreases faster for the smallest precipitate radius of 16 nm and slowest for the largest radius of 21 nm. After 40 min PDG during cooldown, the iron concentration keeps on decreasing and then remains constant. During the first minutes of cooldown, the solid solubility and diffusivity are still high enough so that an appreciable amount of iron is still gettered. When the temperature drops below about 600 °C, the iron concentration in the wafer bulk remains nearly constant. The final iron concentration in the wafer bulk for an as-grown precipitate radius of 16 nm is about one order of magnitude lower than for the larger as-grown radii of 19 and 22 nm.

2.2 Final iron concentration after PDG of varying duration To further investigate the variation in final iron concentration for different as-grown radii, we now look at how the gettering efficacy varies for different process times. In Fig. 2a the post-processed Fe_i concentration is shown as a function of the as-grown precipitate radius for three different gettering times. After the shortest gettering time of 20 min, the post-processed Fe_i concentration decreases with increasing as-grown precipitate radius. After 30 and 40 min PDG, however, it shows a maximum for intermediate precipitate sizes, decreasing strongly for precipitates $\lesssim 17$ nm after 40 min PDG.

Figure 2b shows the corresponding plot of the post-processed total iron concentration as a function of as-grown precipitate radius for three different gettering times. For all gettering times, the total iron concentration decreases with

© 2012 WILEY-VCH Verlag GmbH & Co. KGaA, Weinheim

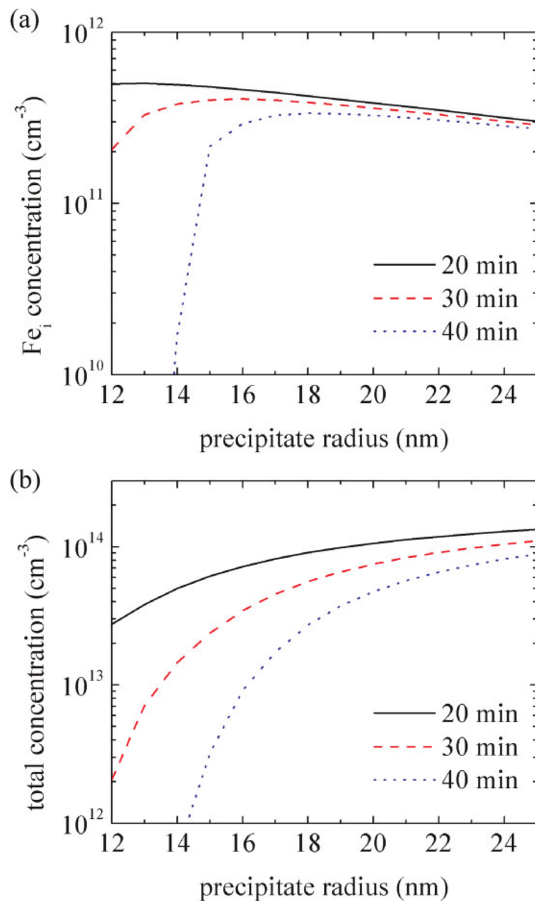

Figure 2 (online color at: www.pss-a.com) Simulated post-gettered (a) Fe_i concentration and (b) total iron concentration in the wafer bulk as a function of as-grown precipitate radius after P diffusion gettering at 840 °C for three different plateau times followed by a 10 min ramp to 800 °C and an exponential cool down to room temperature.

decreasing precipitate radius. This means that the removal of iron from the wafer bulk is faster the smaller the precipitates are for a given initial iron concentration.

3 Experimental Three p-type mc-Si sister wafers of 180 μm thickness and 1.8 $\Omega\,cm^{-1}$ resistivity originating from about 80% up the ingot of a center brick were chemically polished, RCA-cleaned, and dipped in HF. Another sample from the same ingot height was subjected to the same cleaning procedure and ICP-MS was performed to measure the as-grown concentrations of different metals. One sister wafer was subjected to a homogenization step, a 3 min annealing at 950 °C followed by a fast cooldown to room temperature (RT). A second sister wafer was subjected to a ripening step, an extended annealing for 18 h at 740 °C followed by a slow exponential cooldown to RT with a time constant of 210 min. The third wafer remained as-grown. Both annealing steps were conducted in nitrogen atmosphere. Prior to annealing, all quartz glassware including the furnace tube had been cleaned in dilute HF to minimize external contamination.

After annealing, the two annealed wafers were RCA-cleaned and HF-dipped, and all three wafers were silicon nitride (SiN_x)-coated on both sides for surface passivation. The electron lifetime was measured by means of Quasi Steady-State Photoconductance (QSSPC) and the concentration of interstitial iron, Fe_i, was measured via Fe-B pair dissociation [12].

After pre-characterization, SiN_x was removed, wafers were RCA-cleaned and HF-dipped again, and the three sister wafers, the homogenized, the as-grown, and the ripened sample were subjected to PDG at 840 °C during 40 min followed by a 10 min ramp down to 800 °C and finally, an exponential cooldown to RT. Finally, the P emitter was etched off, wafers were RCA-cleaned again, SiN_x-coated on both sides and the final electron lifetime and Fe_i concentration were measured.

4 Experimental results ICP-MS measurements revealed that iron is the predominant metal impurity in the mc-Si under investigation, while Cr, Ni, and Cu were detected in lower concentrations. A total iron concentration of $2.2 \times 10^{14}\,cm^{-3}$ was measured in the as-grown sample, while only $2.6 \times 10^{11}\,cm^{-3}$ of iron was measured to be present in interstitially dissolved form.

The effective electron lifetime measured on the as-grown sister wafer was 37 μs, while somewhat lower lifetimes of 18 and 26 μs were measured on the homogenized and on the ripened sister samples, respectively. After PDG, the electron lifetime on all samples increased, up to 58 μs on the previously as-grown sample, and up to 46 and 48 μs on the previously homogenized and ripened sample, respectively.

Figure 3 shows the Fe_i concentrations measured before (dark blue) and after PDG (turquois). In comparison to the as-grown sister wafer, a higher Fe_i concentration of $5.1 \times 10^{11}\,cm^{-3}$ was measured on the homogenized sample

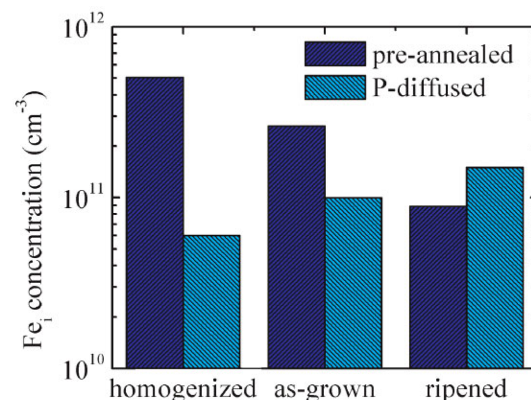

Figure 3 (online color at: www.pss-a.com) Interstitial iron concentration measured on the homogenized, the as-grown, and the ripened mc-Si sister wafer before (dark blue) and after (turquois) 40 min PDG at 840 °C.

© 2012 WILEY-VCH Verlag GmbH & Co. KGaA, Weinheim

and a lower concentration of 9×10^{10} cm^{-3} on the ripened sample after pre-annealing but before PDG. After PDG, the trend is reversed: the lowest Fe_i concentration of 6×10^{10} cm^{-3} was measured on the previously homogenized sample, the next highest concentration of 1×10^{11} cm^{-3} was measured on the previously as-grown sample and the highest concentration of 1.5×10^{11} cm^{-3} was measured on the previously ripened sample.

5 Discussion The aim of the reported experiment was to create three different average size distributions of iron-silicide precipitates in three otherwise very similar wafers, containing the same total amount of iron. Two different pre-annealing steps were performed on two different mc-Si sister wafers and a third sister wafer remained as-grown. On the first sister wafer a homogenization step was performed at 950 °C where the solid solubility of iron is 1.4×10^{14} cm^{-3} [11]. Since the solid solubility is close to the total iron concentration in the material at this temperature, the majority of iron silicide precipitates are assumed to dissolve. During fast cooldown to room temperature, iron is assumed to either remain in interstitially dissolved form or that a high density of very small precipitates forms. The dissolution of more than 50% of metal silicide precipitates during a 20 s annealing at 1000 °C has been previously observed by Buonassisi et al. through μ-XRF analysis [13]. As shown in Fig. 3, an increased Fe_i concentration was actually measured on the homogenized sample in comparison to the as-grown sample. However, the Fe_i concentration is still far below the total iron concentration of 2.2×10^{14} cm^{-3} in the sample. This indicates that dissolution of iron-silicide precipitates took place during high-temperature annealing but that most of the dissolved iron re-precipitated during the fast cooldown, presumingly in a larger density of smaller precipitates.

The second sister wafer was annealed at 740 °C, a temperature at which the solubility limit of iron was recently reported to be around 1×10^{12} cm^{-3} [14], *i.e.*, well below the total concentration of iron in the wafers. During the 18 h annealing at 740 °C, Ostwald ripening is presumed to occur [15], meaning that small iron-silicide precipitates dissolve while larger precipitates grow. As a result, the average precipitate size in the second sister wafer is assumed to increase while the density of precipitates decreases. Figure 3 shows that a decreased Fe_i concentration was measured on the second sister wafer after ripening. This reduction might be due to an internal gettering of iron interstitials to iron-silicide precipitates or crystalline defects during slow cooling.

After 40 min PDG, the lowest Fe_i concentration is measured on the previously homogenized sister wafer and the highest Fe_i concentration is measured on the previously ripened sample. This means that the interstitial iron concentration decreases with decreasing precipitate size, assuming that we successfully engineered precipitate size distributions during pre-annealing. This experimental trend is consistent with simulation results shown in Fig. 2a for as-grown precipitate radii $\lesssim 18$ nm. As-grown radii roughly between 7 and 30 nm and a median value of about 17 nm have been found experimentally in mc-Si wafers [16].

Despite of the lower Fe_i concentration in the previously homogenized samples after PDG, the electron lifetime was not improved over the lifetime in previously as-grown samples. This indicates that the lifetime in these wafers was not limited by interstitial iron after PDG. However, we expect the behavior of Fe_i demonstrated here to apply in cases where the wafer *is* limited by Fe_i after PDG. Many industrial PDG processes are significantly shorter than the one applied here which increases the relative importance of Fe_i after processing as seen in Fig. 2a.

The observed trend in the Fe_i concentration after PDG can be explained when comparing its the evolution for different as-grown precipitate radii shown in Fig. 1a: it is observed that the highest quasi steady-state equilibrium Fe_i concentration establishes for the smallest as-grown precipitate radius of 16 nm (solid line). The dissolution effect is stronger for smaller precipitates due to larger surface-to-volume ratio. However, as shown in Fig. 1b the faster dissolution of small precipitates also allows a faster reduction of total iron concentration in the wafer bulk, leading to a steeper decrease of the Fe_i concentration with time. After a certain gettering time between 35 and 40 min as seen in Fig. 1a, there is a cross-over point where the average bulk Fe_i concentration for smaller as-grown precipitates drops below the Fe_i concentration for larger as-grown precipitate sizes.

Our findings may help to understand precipitate kinetics during high temperature processing and to customize the time-temperature profile of PDG to as-grown materials. As mentioned in the introduction, a high density of small precipitates, comparable to the homogenized sample in our experiment, is usually found in Si ribbon materials directly grown from the melt. In these types of materials, a longer PDG time or higher temperature might be beneficial for a more complete removal of iron from the wafer. In ingot-grown samples with larger precipitates, however, a much longer PDG step would be necessary for complete iron removal. Therefore, a longer high-temperature plateau during PDG does not seem to have a large impact on improving material performance. As first suggested by Plekhanov et al. [8], later by Seibt et al. [17], and recently tested experimentally by Schön et al. [18], a two-step variable temperature profile might be beneficial in some cases: the emitter formation is performed in a shorter time at higher temperature in order dissolve all precipitates while longer time is spent for cooldown or low temperature annealing, during which the Fe_i concentration is decreased significantly.

6 Conclusions Simulations and experimental results indicate that the reduction of the precipitated and interstitial iron concentration during PDG strongly depends on the precipitate size distribution. Smaller precipitates dissolve faster and therefore, in Si materials with smaller as-grown precipitate size, this may result in a higher Fe_i concentration

© 2012 WILEY-VCH Verlag GmbH & Co. KGaA, Weinheim

if gettering is incomplete. However, a complete removal of iron from the wafer bulk in these materials is potentially possible if the gettering time is long enough.

Acknowledgements This material is based upon work primarily supported by the National Science Foundation (NSF) and the Department of Energy (DOE) under NSF CA No. EEC-1041895. The work was partially funded by the Spanish Ministerio de Ciencia e Innovación through Thincells (TEC2008–06798–C03–02) and Crysthin (TEC2011–28423–C03) projects. SiN_x depositions were performed at the Center for Nanoscale Systems (CNS), a member of the National Nanotechnology Infrastructure Network (NNIN), which is supported by the National Science Foundation under NSF award no. ECS-0335765. CNS is part of Harvard University. J. Hofstetter acknowledges the support of the Alexander von Humboldt foundation through a Feodor Lynen Fellowship. D. P. Fenning acknowledges the support of the National Science Foundation Graduate Research Fellowship.

References

[1] D. M. Powell, M. T. Winkler, H. J. Choi, C. B. Simmons, D. B. Needleman, and T. Buonassisi, Energy Environ. Sci. **5**, 5874–5883 (2012).
[2] S. McHugo, H. Hieslmair, and E. Weber, Appl. Phys. A **64**, 127–137 (1997).
[3] S. Peters, J. Lee, C. Ballif, D. Borchert, S. Glunz, W. Warta, and G. Willeke, Rapid thermal processing: a comprehensive classification of silicon materials, in: Photovoltaic Specialists Conference, 2002, Conference Record of the 29th IEEE (May 2002), pp. 214–217
[4] A. A. Istratov, T. Buonassisi, R. J. McDonald, A. R. Smith, R. Schindler, J. A. Rand, J. P. Kalejs, and E. R. Weber, J. Appl. Phys. **94**, 6552–6559 (2003).
[5] G. Hahn and A. Schönecker, J. Phys.: Condens. Matter **16**(50), R1615. (2004).
[6] T. Buonassisi, A. A. Istratov, M. Heuer, M. A. Marcus, R. Jonczyk, J. Isenberg, B. Lai, Z. Cai, S. Heald, W. Warta, R. Schindler, G. Willeke, and E. R. Weber, J. Appl. Phys. **97**, 074901-1–074901–11 (2005).
[7] A. Haarahiltunen, H. Savin, M. Yli-Koski, H. Talvitie, M. Asghar, and J. Sinkkonen, Mater. Sci. Eng. B **159/160**, 248–252 (2009).
[8] P. S. Plekhanov, R. Gafiteanu, U. M. Gösele, and T. Y. Tan, J. Appl. Phys. **86**, 2453–2458 (1999).
[9] J. Hofstetter, D. P. Fenning, M. I. Bertoni, J. F. Lelièvre, C. del Cañizo, and T. Buonassisi, Prog. Photovolt. Res. Appl. **19**, 487–497 (2011).
[10] Impurities-to-Efficiency (I2E) simulator, online applet, http://pv-i2e.mit.edu.
[11] M. Aoki, A. Hara, and A. Ohsawa, J. Appl. Phys. **72**, 895–898 (1992).
[12] D. H. Macdonald, L. J. Geerligs, and A. Azzizi, J. Appl. Phys. **95**(3), 1021–1028 (2004).
[13] T. Buonassisi, A. Istratov, S. Peters, C. Ballif, J. Isenberg, S. Riepe, W. Warta, R. Schindler, G. Willeke, Z. Cai, B. Lai, and E. R. Weber, Appl. Phys. Lett. **87**, 121918 (2005).
[14] J. D. Murphy and R. J. Falster, Phys. Status Solidi RRL **5**(10–11), 370–372 (2011).
[15] X. W. Lin, J. Washburn, and Z. Liliental-Weber, J. Appl. Phys. **75**, 4686 (1994).
[16] D. P. Fenning, J. Hofstetter, M. I. Bertoni, S. Hudelson, M. Rinio, J. F. Lelièvre, B. Lai, C. del Cañizo, and T. Buonassisi, Appl. Phys. Lett. **98**, 162103 (2011).
[17] M. Seibt, A. Sattler, C. Rudolf, O. Voss, V. Kveder, and W. Schröter, Phys. Status Solidi A **203**, 696 (2006).
[18] J. Schön, H. Habenicht, M. Schubert, and W. Warta, J. Appl. Phys. **109**, 063717 (2011).

© 2012 WILEY-VCH Verlag GmbH & Co. KGaA, Weinheim